UNIVERSITY
OF TRENTO

DIPARTIMENTO DI INGEGNERIA E SCIENZA DELL'INFORMAZIONE

38123 Povo – Trento (Italy), Via Sommarive 14
http://www.disi.unitn.it

ELECTROMAGNETIC PASSIVE LOCALIZATION AND TRACKING OF MOVING TARGETS IN A WSN-INFRASTRUCTURED ENVIRONMENT

F. Viani, P. Rocca, M. Benedetti, G. Oliveri, and A. Massa

January 2011

Technical Report # DISI-11-100

Electromagnetic Passive Localization and Tracking of Moving Targets in a WSN-Infrastructured Environment

F. Viani, P. Rocca, M. Benedetti, G. Oliveri, and A. Massa

Department of Information Engineering and Computer Science,

University of Trento, Via Sommarive 14, 38123 Trento - Italy

Tel. +39 0461 882057, Fax +39 0461 882093

E-mail: *andrea.massa@ing.unitn.it,*

{*federico.viani, paolo.rocca, manuel.benedetti, giacomo.oliveri*}@*disi.unitn.it*

Web-site: *http://www.eledia.ing.unitn.it*

Electromagnetic Passive Localization and Tracking of Moving Targets in a WSN-Infrastructured Environment

F. Viani, P. Rocca, M. Benedetti, G. Oliveri, and A. Massa

Abstract

In this paper, an innovative strategy for passive localization of transceiver-free objects is presented. The localization is yielded by processing the received signal strength data measured in an infrastructured environment. The problem is reformulated in terms of an inverse source one, where the probability map of the presence of an equivalent source modeling the moving target is looked for. Towards this end, a customized classification procedure based on a support vector machine is exploited. Selected, but representative, experimental results are reported to assess the feasibility of the proposed approach and to show the potentialities and applicability of this passive and unsupervised technique.

Key words: Object tracking, wireless sensor networks, transceiver-free objects, received signal strength indicator, classification problem, support vector machine.

1 Introduction

In the recent years, there has been a wide and rapid diffusion of wireless sensor networks (WSNs) [1] thanks to the availability of such low-power and pervasive devices integrating on-board sensing, processing, and radio frequency (RF) circuitry for information transmission. Usually, short-range communications are at hand since the wireless nodes are generally densely distributed and characterized by low power consumption to ensure a long lifetime. Therefore, WSNs have been also profitably used for location and tracking purposes. In such a framework, the main efforts have been devoted to develop ad-hoc systems based on dedicated transponders/sensors [2] or assuming an "active" target equipped with a transmitting device [3][4]. Different properties of the received signal, such as the time of arrival (TOA) and the direction of arrival (DOA), have been successfully exploited to address the localization problem [5][6]. Other modalities to locate active targets are based on the evaluation of the received signal strength (RSS) [7][8][9][10]. This is an easily measurable quantity that has been also used to localize the wireless nodes of the network through effective triangulation strategies [8]. Moreover, the distance between nodes has been estimated thanks to simplified radio propagation models. Although easier than a "passive" localization technique, the main drawback of these approaches is the need of the target to be equipped with an ad-hoc device. Whether such a fact can be considered negligible when tracking either objects or animals (although the costs unavoidably increase), other problems arise when dealing with people (e.g., privacy) and especially with non-cooperative subjects as for elderly people. Moreover, such wearable devices can undergo (casual or voluntary) damages thus limiting the reliability of the tracking system. Other strategies concerned with transceiver-free targets have been also presented in the scientific literature. State-of-the-art approaches are based on Doppler radar systems able to estimate the distance between the target and the sensor [11]. As a matter of fact, moving targets can be tracked through the analysis of the Doppler signature induced by the object motion [12]. Unfortunately, the arising performance in real environments can be strongly influenced by non-negligible instabilities leading to several false alarms. Furthermore, slow-moving targets [13] are not generally detected.

This paper is aimed at presenting an inversion procedure, preliminary validated in [14], for the localization and tracking of passive objects starting from the measurements of the RSS indexes available at the nodes of a WSN. Since the transmission of information among the wireless nodes is allowed by RF signals, the arising electromagnetic radiations can be also profitably exploited to sense the surrounding environment. Indeed, any target lying within the environment interacts with the electromagnetic waves radiated by the nodes. Therefore, the measurements of the perturbation effects on the other receiving nodes is dealt with a suitable inversion strategy to determine the equivalent source modeling the presence of the target/scatterer generating the perturbation itself. By virtue of the fact that the number of nodes in a WSN can vary and the need to have a simple and flexible tracking/localization method allowing real-time estimates, a learning-by-examples (LBE) strategy based on a Support Vector Machine (SVM) is used. Although only recently applied for the solution of electromagnetic inverse problems, effective approaches based on learning-by-examples techniques have been already proposed for the estimation of the direction of arrival of desired/undesired signals [15][16], the detection of buried objects [17][18][19], and the early beast cancer imaging [20] thanks to their efficiency and versatility.

The outline of the paper is as follows. The mathematical issues concerned with the proposed approach are detailed in Sect. 2 where the SVM-based method is described, as well. In Sect. 3, representative results from a wide set of experiments dealing with the tracking of single as well as multiple targets in both outdoor and indoor WSN deployments are shown. Eventually, some conclusions are drawn (Sect. 4).

2 Mathematical Formulation

Let us consider the two-dimensional ($2D$) scenario shown in Fig. $1(a)$. The investigation domain D is inhomogeneous and constituted by a set of obstacles and moving targets to be localized/tracked all lying in free-space. The known host scenario (i.e., the target-free domain) is described by the object function $\tau_h(\underline{r}) = \varepsilon_h(\underline{r}) - 1 - j\frac{\sigma_h(\underline{r})}{\omega\varepsilon_0}$ where ω is the working angular frequency, $\underline{r} = (x, y)$ is the position vector, ε_h and σ_h being the dielectric

permittivity and the conductivity, respectively. Moreover, the target/s is/are identified by the dielectric distribution $\tau_o(\underline{r})$, $\underline{r} \in D_o$. The area under test is infrastructured with a WSN and S nodes are deployed at $\underline{r}_s$, $s = 1, ..., S$ spatial locations. The s-th wireless node radiates an electromagnetic signal, $\xi_s^{inc}(\underline{r})$ [(1)], and the field measured by the other $S-1$ nodes and arising from the interactions of the incident field with the scenario under test is given by

$$\xi_s^{tot}(\underline{r}_m) = \xi_s^{inc}(\underline{r}_m) + \int_D J(\underline{r}')\,\mathcal{G}_0(\underline{r}', \underline{r}_m)\,d\underline{r}' \tag{1}$$

where $\mathcal{G}_0$ is the free-space Green's function [21] and $\underline{r}_m$ is the position of the m-th ($m = 1, ..., S-1$) receiving node. As a matter of fact, the field induced in D is equivalent to that radiated in free-space by an equivalent current density $J(\underline{r}) = \tau(\underline{r})\,\xi^{tot}(\underline{r})$, $\underline{r} \in D$ [22] modeling the presence of whatever discontinuity of the free-space (i.e., both the obstacles and the moving targets) where $\tau(\underline{r}) = \tau_o(\underline{r})$ if $\underline{r} \in D_o$ and $\tau(\underline{r}) = \tau_h(\underline{r})$ if $\underline{r} \in D_h = D - D_o$, D_o and D_h being the support of the targets and its complementary area.

Equation (1) can be reformulated in a different fashion by defining a differential equivalent current density $\hat{J}(\underline{r})$ radiating in the inhomogeneous host medium [21] [Fig. $1(b)$]. Since the host medium is *a-priori* known, the radiated field can be then expressed as

$$\xi_s^{tot}(\underline{r}_m) = \hat{\xi}_s^{inc}(\underline{r}_m) + \int_{D_o} \hat{J}(\underline{r}')\,\mathcal{G}_1(\underline{r}', \underline{r}_m)\,d\underline{r}' \tag{2}$$

where

$$\hat{\xi}_s^{inc}(\underline{r}_m) = \xi_s^{inc}(\underline{r}_m) + \int_D \tau_h(\underline{r}')\,\xi_{s,u}^{tot}(\underline{r}')\,\mathcal{G}_0(\underline{r}', \underline{r}_m)\,d\underline{r}' \tag{3}$$

is the field of the scenario without targets and equivalent to an "incident" field on the targets, $\hat{J}(\underline{r}) = \hat{\tau}(\underline{r})\,\xi_{s,p}^{tot}(\underline{r})$ and $\hat{\tau}(\underline{r}) = \tau(\underline{r}) - \tau_h(\underline{r})$ is the differential object function. In (3), the second term on the right side is the field scattered from the host medium without targets, $\xi_{s,u}^{tot}$ being the electric field related to ξ_s^{inc} in correspondence with the

[(1)] The scalar case has been considered to simplify the notation. However, the extension to the vectorial case is straightforward.

target-free scenario. Moreover, $\mathcal{G}_1$ is the inhomogeneous Green's function for the target-free configuration [21], which satisfies the following integral equation

$$\mathcal{G}_1\left(\underline{r},\underline{r}'\right)=\mathcal{G}_0\left(\underline{r},\underline{r}'\right)+\int_D \tau_h\left(\underline{r}'\right)\mathcal{G}_0\left(\underline{r},\underline{r}"\right)\mathcal{G}_1\left(\underline{r}",\underline{r}'\right)d\underline{r}". \tag{4}$$

With the knowledge of $\mathcal{G}_1$ (i.e., the knowledge of the target-free scenario) the scattering problem turns out to be the retrieval of the differential source $\hat{J}$ occupying the target domain D_o. The detection of the target position and the definition of the target trajectory in D can be then formulated as the definition of the support of the differential equivalent source, which satisfies the inverse scattering equation (2), starting from the measurements of $\xi^{tot}\left(\underline{r}_m\right)$, $m=1,...,S-1$. This is possible in a WSN-infrastructured environment since the nodes at hand are simple and cheap devices that give an indirect estimate of the field value through the RSS index. Accordingly, the RSS is measured at the m-th node when the s-th node is transmitting by considering both the target-free scenario [$\xi_s^{inc}\left(\underline{r}_m\right)$ knowledge] and the presence of targets within D [$\xi_s^{tot}\left(\underline{r}_m\right)$ knowledge] and the differential field $\xi_{m,s}^{sct}=\xi_s^{tot}\left(\underline{r}_m\right)-\hat{\xi}_s^{inc}\left(\underline{r}_m\right)$ could be used for the inversion procedure.

However, it is worth to take into account that the power radiated by the WSN nodes can vary due to several factors (e.g., battery level of the WNS nodes, environmental conditions) thus "blurring" the data acquisition and, consequently, complicating the solution of the inverse problem at hand. To overcome this drawback, the inversion is statistically recast as the definition of the probability that a target is located in a position of D starting from the knowledge of $\xi_{m,s}^{sct}$, $s=1,...,S$, $m=1,...,S$, $m\neq s$. The arising classification problem is then solved by means of a suitable SVM-based approach. Such a strategy allows one to improve the generalization capability of the localization and tracking system since it is less sensitive to the instantaneous variations of the measurements by virtue of the underlying probabilistic model. Moreover, it is also able to deal with scenarios not considered in the training phase as well as to perform the real time tracking of multiple targets. More specifically, the proposed approach works as follows. The region D where the targets are looked for is partitioned into a grid of C cells centered at $\underline{r}_c$, $c=1,...,C$. Each c-th cell is characterized by its state, χ_c, which can be either empty ($\chi_c=-1$) or

occupied ($\chi_c = 1$) whether a target (i.e., the corresponding differential equivalent source) is present or absent. Moreover, the probability that a target belongs to the c-th cell, $\alpha_c = Pr\{\chi_c = 1 | (\underline{\Gamma}, c)\}$, is given by

$$\alpha_c = \frac{1}{1 + exp\left\{p\mathcal{H}\left[\underline{\varphi}(\underline{\Gamma}, c)\right] + q\right\}}, \quad c = 1, ..., C \tag{5}$$

where $\underline{\Gamma} = \left\{\xi_{m,s}^{sct};\ s = 1, ..., S;\ m = 1, ..., S;\ m \neq n\right\}$, and p, q are unknown parameters to be determined [23]. In (5), the function $\underline{\varphi}(\cdot)$ is a non-linear mapping from the data of the original input space, $\underline{\Gamma}$, to a higher dimensional space (called *feature space*) where the data are more easily separable through a simpler function (i.e., the hyperplane $\mathcal{H}$).

The hyperplane $\mathcal{H}$ is off-line defined throughout the *training phase* by exploiting the knowledge of a set of T known examples where both the input data ($\underline{\Gamma}$, $t = 1, ..., T$) and the corresponding maps ($\underline{\chi}_t = \{\chi_{c,t};\ c = 1, ..., C\}$, $t = 1, ..., T$) are available. Usually, a linear decision function is adopted

$$\mathcal{H}\left[\underline{\varphi}(\underline{\Gamma}, c)\right] = \underline{w} \cdot \underline{\varphi}(\underline{\Gamma}, c) + b, \quad c = 1, ..., C \tag{6}$$

$\underline{w}$ and b being an unknown normal vector and a bias coefficient, respectively.The decision function parameters unequivocally define the decision plane and are computed in the training phase by minimizing the following cost function

$$\Psi(\underline{w}) = \frac{\|\underline{w}\|^2}{2} + \frac{\lambda}{\sum_{t=1}^{T} C_+^{(t)}} \sum_{t=1}^{T} \sum_{c=1}^{C_+^{(t)}} \eta_{c+}^{(t)} + \frac{\lambda}{\sum_{t=1}^{T} C_-^{(t)}} \sum_{t=1}^{T} \sum_{c=1}^{C_-^{(t)}} \eta_{c-}^{(t)} \tag{7}$$

subject to the separability constraints

$$\begin{aligned} &\underline{w} \cdot \underline{\varphi}(\underline{\Gamma}, c) + b \geq 1 - \eta_{c+}^{(t)}, \quad c = 1, ..., C \\ &\underline{w} \cdot \underline{\varphi}(\underline{\Gamma}, c) + b \leq \eta_{c-}^{(t)} - 1, \quad c = 1, ..., C \end{aligned} \tag{8}$$

where λ is a user-defined hyperparameter [24] that controls the trade-off between the training error and the model complexity to avoid overfitting. Moreover, $\eta_{c+}^{(t)}$ and $\eta_{c-}^{(t)}$ are the so-called *slack variables* related to the misclassified patterns. They are introduced because the training data are usually not completely separable in the feature space by

means of a linear hyperplane.

The minimization of (7) is performed following the guidelines detailed in [17] and also exploiting the so-called kernel trick method [23].

3 Experimental Validation

The feasibility and the effectiveness of the proposed approach have been assessed through an extensive experimental validation carried out in both indoor and outdoor scenarios (Fig. 2). The nodes have been placed at fixed positions $\underline{r}_s = (x_s, y_s)$, $s = 1, ..., S$, on the perimeter of the investigation area D. In all experiments, the region D has been assumed having the same size ($-20\lambda \leq x \leq 20\lambda$ and $-12\lambda \leq y \leq 12\lambda$) whatever the scenario at hand, λ being the free-space wavelength of the wireless signals transmitted by the nodes (e.g., $f = 2.4\,GHz$), and $S = 6$ Tmote Sky nodes have been used to obtained a suitable trade-off between the complexity of the sensor network (i.e., the number of sensor nodes) and the efficiency of the system (i.e., the sampling rate) while guaranteeing a complete coverage of D (i.e., each sensor node is connected at least to another node of the network in case of target-free scenario). Although the same topology has been adopted for outdoor as well as indoor situations, two different trainings of the SVM-based approach have been performed since the arising electromagnetic phenomena significantly differ (e.g., the electromagnetic interferences). Otherwise, the calibration of training examples (T), the separation hyperplane $\mathcal{H}$ (λ), and the discretization of the investigation area (C) has been performed only once, namely for the outdoor case, since the format of the data processed by the SVM does not change. More in detail, the following setup has been considered: $T \in [100, 700]$ with step $\Delta T = 100$, $\lambda = 10^i$, $i = \{0, 1, 2, 3\}$, and $C \in [15, 960]$ from a rough discretization with $C = 5 \times 3$ cells of dimension $4\lambda \times 4\lambda$ to the finest one having $C = 40 \times 24$ cells of dimension $\lambda \times \lambda$. These values have been calibrated with reference to single-target experiments by evaluating the behavior of the localization error defined as

$$\rho = \frac{\sqrt{\left(x_j^{act} - x_j^{est}\right)^2 + \left(y_j^{act} - y_j^{est}\right)^2}}{\rho_{max}} \tag{9}$$

where $\underline{r}_j^{act} = \left(x_j^{act}, y_j^{act}\right)$ and $\underline{r}_j^{est} = \left(x_j^{est}, y_j^{est}\right)$ are the actual and estimated positions of the

target, ρ_{max} being the maximum admissible location error. As for the test case at hand, it turns out that $\rho_{max} = \sqrt{X_D^2 + Y_D^2}$ and $\underline{r}_j^{est}$ has been calculated from the probability map according to the following relationships

$$\begin{aligned} x_j^{est} &= \frac{\sum_{c=1}^{C} \alpha_c x_c}{\sum_{c=1}^{C} \alpha_c} \\ y_j^{est} &= \frac{\sum_{c=1}^{C} \alpha_c y_c}{\sum_{c=1}^{C} \alpha_c}. \end{aligned} \tag{10}$$

Figure 3 gives the normalized values of the location indexes obtained for different combinations of the control parameters. Each plot refers to the variation of a control parameter keeping constant the others ($T^{opt} = 500$, $\lambda^{opt} = 100$, $C^{opt} = 60$).

As far as the SVM training phase is concerned, the reference measurements have been first collected in the target-free scenarios [i.e., $\hat{\tau}(\underline{r}) = 0 \Rightarrow \xi_{m,s}^{sct} = 0$, $m, s = 1, ..., S$, $m \neq s$]. Successively, the sets of RSS measurements [i.e., $RSS_{m,s}(t)$, $m, s = 1, ..., S$, $m \neq s$, $t = 1, ..., T$] have been collected with the target located at T different positions, $\underline{r}_j = (x_j, y_j)$, $j = 1, .., T$, randomly selected within D to cover as uniformly as possible the whole area under test. Concerning the required computational time, the burden of the training phase grows proportionally with the number of training samples and the discretization of D from a minimum of 3×10^2 $[s]$ when $T = 100$, $C = 15$ up to a maximum of 10^4 $[s]$ (i.e., almost three hours) when $T = 700$, $C = 960$.

As regards the SVM test step, both single ($J = 1$) and multiple ($J = 2$) target tracking problems have been considered. Since off-the-shelf sensor nodes are used for these experiments, they allow to obtain one RSS measurement each 5×10^{-2} $[s]$. Therefore, considering the situation where each node has to collect a RSS measurement for all other $S - 1$ nodes, the maximum acquisition time is 2 $[s]$. The system is then able to process the data and define a localization map α_c, $c = 1, ..., C$, in 0.1 $[s]$ using a $3\,GHz$ PC with $2\,GB$ of RAM.

The first experiment deals with the outdoor tracking of a single human being moving inside D. Figure 4 shows the probability map estimated when the target is at $\underline{r}_1^{act} = (-16\lambda, 8\lambda)$.

The circle gives the actual position. Two different cases have been considered. More specifically, Figure 4(a) shows the probability map assuming that the same experiment has been taken into account in the training phase. Differently, the map in Fig. 4(b) has been obtained the example not belonging to the training data set. It is worth noting that the target is correctly localized in both maps since the center of the target lies within the region with higher probability. The same experiment has been successively considered for the indoor scenario. The results of the SVM-based localization process are shown in Fig. 5. As for the previous test, the results when the same example has been either considered [Fig. 5(a)] or not [Fig. 5(b)] in the training phase have been reported. As expected, the values of the localization errors increase whatever the training because of the complexity of the electromagnetic interactions arising from the presence of the walls (i.e., multiple reflections) in indoor environments. Nevertheless, the region with high probability still contains the actual position of the target thus demonstrating a good degree of reliability of the approach also in this case.

Let us now consider a single target moving outdoor inside D along the straight line shown in Fig. 6. The RSS values have been measured at 6 different time instants, but it is worth to point out that the acquisition time can be further shortened to reach an almost real-time tracking. The samples of the localization maps and the estimated path are reported in Fig. 7 and Fig. 6, respectively. As it can be observed, there is a good matching between the actual path and the estimated one assessing the effectiveness of the approach in real-time processing, as well. The same analysis has been carried out for the indoor case. Although the moving target is quite carefully localized, the result in Figure 8 and the location indexes in Tab. I confirm the higher complexity of tracking the target as compared to the outdoor case.

In order to deal with the tracking of multiple targets, the SVM classifier has been trained with a mixed data-set containing examples with one (T_1 examples with $J = 1$) and two (T_2 examples with $J = 2$) targets. Since $T = T_1 + T_2$ examples have been used also for the single-target training, some experiments have been carried out to analyze the dependence of the localization on the percentage of training samples from T_1 and T_2. The probability

maps in Fig. 9 show that the position of one target can be correctly located although a smaller set of single-target examples has been used for the training phase (i.e., $T_1 < T_2$). Vice versa, a larger number of example is needed for an effective localization of the two targets as pointed out by the maps in Fig. 10 and quantified by the location indexes in Tab. II. Such a behavior was expected since the number of different combinations with two targets is higher if compared to the single-target case. Therefore, $T_1 = 150$ and $T_2 = 350$ examples have been successively used for the training phase of the following tracking experiments.

As representative examples, two different situations with $J = 2$ have been dealt with. In the former, one target ($j = 1$) is moving within D while the other ($j = 2$) remains immobile in the same position. Instead, both targets are moving in the second example. The actual trajectory and the estimated one are shown in Fig. 11 and Fig. 12, respectively. Whatever the example at hand, a quite careful indication on the position and path followed by the targets has been obtained as further confirmed by the average values of the localization errors (outdoor: $\overline{\rho}_1 = 0.070$, $\overline{\rho}_2 = 0.061$ - indoor: $\overline{\rho}_1 = 0.101$, $\overline{\rho}_2 = 0.070$).

4 Conclusions

In this work, the localization and tracking of passive targets have been addressed by exploiting the RSS values available at the nodes of a WSN. The problem at hand has been reformulated into an inverse source one aimed at reconstructing the support of an equivalent source generating a perturbation of the wireless links among the WSN nodes equal to that due to the presence of targets within the monitored area. The inversion has been faced with a learning-by-examples approach based on a SVM classifier devoted to determine a map of the *a-posteriori* probability that a differential equivalent source is present within the investigation domain. Experimental results have assessed the effectiveness and reliability of the proposed approach in dealing with the tracking of single and multiple human beings both in indoor and outdoor environments.

References

[1] C.-Y. Chong and S. P. Kumar, "Sensor networks: evolution, opportunities, and challenges," *Proc. IEEE*, vol. 91, no. 8, pp. 1247-1256, Aug. 2003.

[2] Z. Li, W. Dehaene, and G. Gielen, "A 3-tier UWB-based indoor localization system for ultra-low-power sensor networks" *IEEE Trans. Wireless Commun.*, vol. 8 , no. 6, pp. 2813-2818, Jun. 2009.

[3] G. Latsoudas and N. D. Sidiropoulos, "A fast and effective multidimensional scaling approach for node localization in wireless sensor networks," *IEEE Trans. Geosci. Remote Sens.*, vol. 55, no. 10, pp. 5121-5127, Oct. 2007.

[4] C.-T. Huang, C.-H. Wu, Y.-N. Lee and J.-T. Chen, "A novel indoor RSS-based position location algorithm using factor graphs," *IEEE Trans. Wireless Commun.*, vol. 8, no. 6, pp. 3050-3058, Jun. 2009.

[5] K. Pahlavan, X. Li, and J. P. Makela, "Indoor geolocation science and technology," *IEEE Commun. Mag.*, vol. 40, no. 2, pp. 112-118, Feb. 2002.

[6] A. Catovic, and Z. Sahinoglu, "The Cramer-Rao bounds of hybrid TOA/RSS and TDOA/RSS location estimation schemes," *IEEE Commun. Lett.*, vol. 8, no. 10, pp. 626-628, Oct. 2004.

[7] X. Li, "RSS-based location estimation with unknown pathloss model," *IEEE Trans. Wireless Commun.*, vol. 5, no. 12, pp. 3626-3633, Dec. 2006.

[8] X. Li, "Collaborative localization with received-signal strength in wireless sensor networks," *IEEE Trans. Veh. Technol.*, vol. 56, no. 6, pp. 3807-3817, Nov . 2007.

[9] F. Cabrera-Mora and J. Xiao, "Preprocessing technique to signal strength data of wireless sensor network for real-time distance estimation," *2008 IEEE Int. Conf. Robotics Automation*, Pasadena, CA, USA, May 19-23, 2008, pp. 1537-1542.

[10] M. Saxena, P. Gupta, B. N. Jain, "Experimental analysis of RSSI-based location estimation in wireless sensor networks," *2008 IEEE Conf. Commun. System Software and Middleware (COMSWARE)*, Bangalore, India, pp. 503-510, Jan. 2008.

[11] W. Butler, "Design considerations for intrusion detection wide area surveillance radars for perimeters and borders," *2008 IEEE Int. Conf. Tech. Homeland Security*, Waltham, MA, USA, May 12-13, 2008, pp. 47-50.

[12] A. S. Bugaev, V. V. Chapurski, S. I. Ivashov, V. V. Razevig, A. P. Sheiko, and I. A. Vasilyev, "Through wall sensing of human breathing and heart beating by monochromatic radar," *2004 Int. Conf. Ground Penetrating Radar*, Delft, Netherlands, Jun. 21-24, 2004, vol. 1, pp. 291-294.

[13] P. Withington, H. Fluhler, and S. Nag, "Enhancing homeland security with advanced UWB sensors," *IEEE Microw. Mag.*, vol. 4, no. 3, pp. 51- 58, Sept. 2003.

[14] F. Viani, L. Lizzi, P. Rocca, M. Benedetti, M. Donelli, and A. Massa, "Object tracking through RSSI measurements in wireless sensor networks," *Electron. Lett.*, vol. 44, no. 10, pp. 653-654, 2008.

[15] A. H. El Zooghby, C. G. Christodoulou, and M. Georgiopulos, "A neural network-based smart antenna for multiple source tracking," *IEEE Trans. Antennas Propag.*, vol. 48, no. 5, pp. 768-776, May 2000.

[16] M. Donelli, F. Viani, P. Rocca, and A. Massa, "An innovative multiresolution approach for DOA estimation based on a support vector classification," *IEEE Trans. Antennas Propag.*, vol. 57, no. 8, pp. 2279-2292, Aug. 2009.

[17] A. Massa, A. Boni, and M. Donelli, "A classification approach based on SVM for electromagnetic subsurface sensing," *IEEE Trans. Geosci. Remote Sens.*, vol. 43, no. 9, pp. 2084-2093, Sep. 2005.

[18] Q. Liu, X. Liao, and L. Carin, "Detection of unexploded ordnance via efficient semisupervised and active learning," *IEEE Trans. Geosci. Remote Sens.*, vol. 46, no. 9, pp. 2558-2567, Sep. 2008.

[19] E. Pasolli, F. Melgani, and M. Donelli, "Gaussian process approach to buried object size estimation in GPR images," *IEEE Geosci. Remote Sens. Lett.*, vol. 7, no. 1, pp. 141-145, Sep. 2009.

[20] F. Viani, P. Meaney, P. Rocca, R. Azaro, M. Donelli, G. Oliveri, and A. Massa, "Numerical validation and experimental results of a multiŋresolution SVMŋbased classification procedure for breast imaging," *Proc. 2009 IEEE APŋS Int. Symp.*, Charleston, SC, USA, June 1ŋ5, 2009, pp. 1-4.

[21] W. C. Chew, *Waves and Fields in Inhomogeneous Media*. New York: Van Nostrand Reinhold, 1990.

[22] A. Ishimaru, *Electromagnetic Wave, Propagation, Radiation and Scattering*. Englewood Cliffs, NJ: Prentice-Hall, 1991.

[23] V.Vapnik, *Statistical Learning Theory*. New York, USA: Wiley, 1998.

[24] K. Morik, P. Brockhausen, and T. Joachims, "Combining statistical learning with a knowledge-based approach - A case study in intensive care monitoring," *1999 Int. Conf. Machine Learn. (ICML 1999)*, June 27-30, 1999, Bled, Slovenia, pp. 268-277.

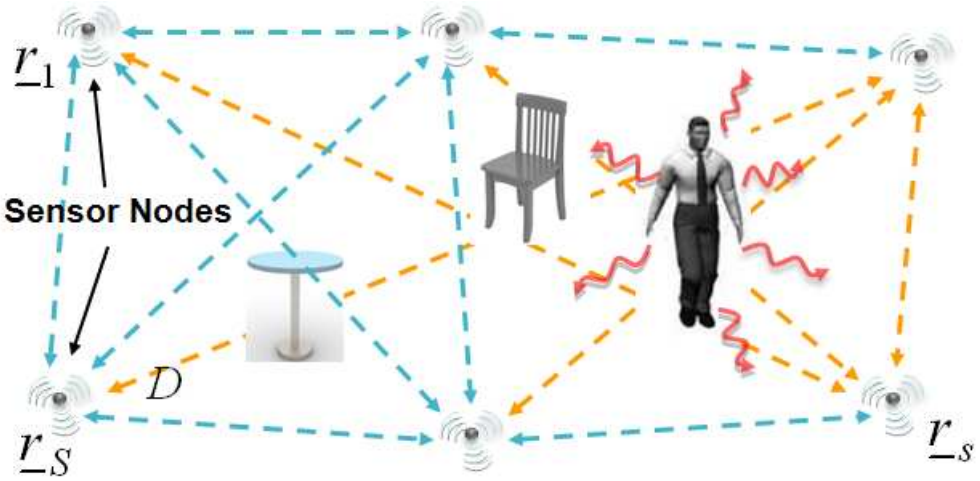

(a)

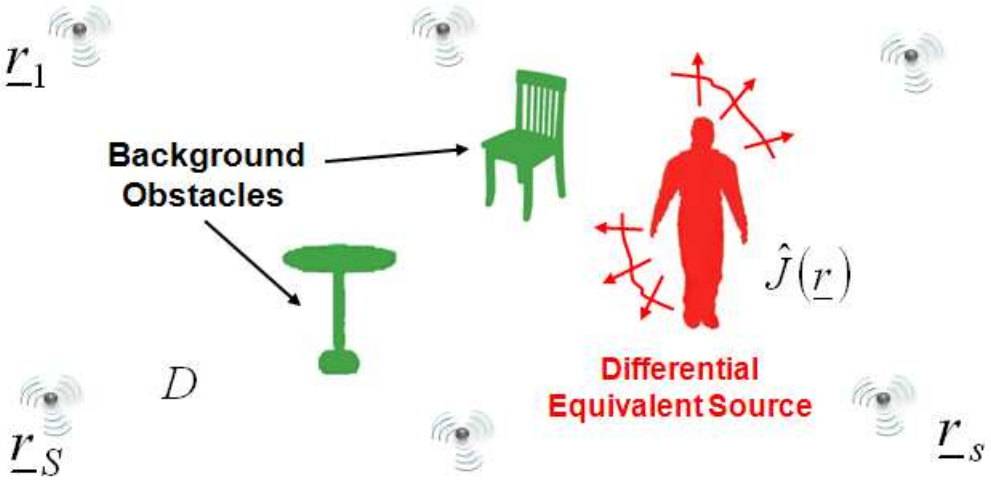

(b)

Fig. 1 - *Equivalent Tracking Problem* - Sketch of (a) the tracking scenario and (b) the equivalent inverse problem.

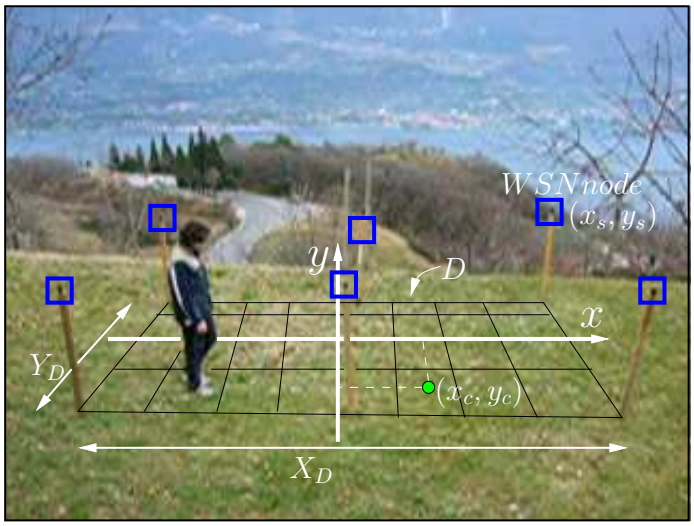

(a)

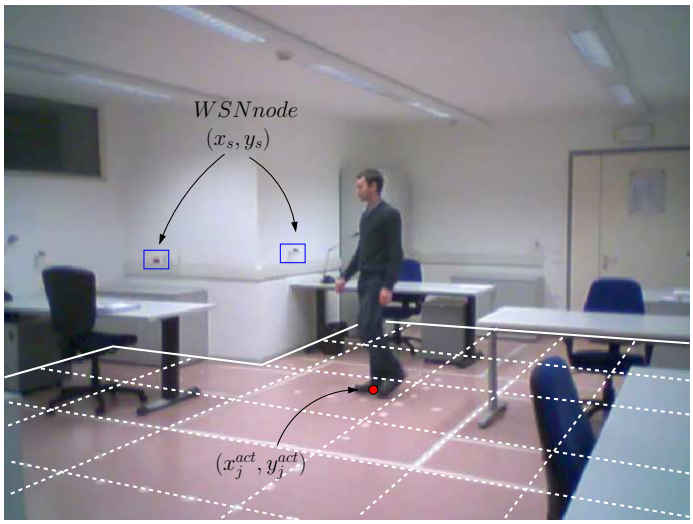

(b)

Fig. 2 - *Problem Geometry* - Plots of (a) the outdoor and (b) the indoor environments with WSN-based tracking system.

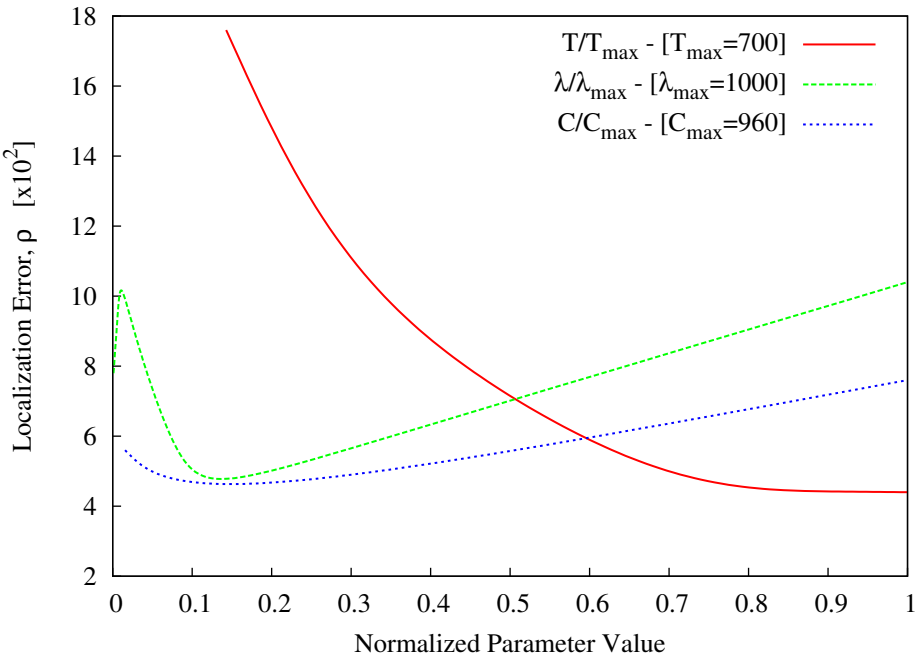

Fig. 3 - *Calibration* - Localization error as a function of the SVM control parameters: T ($\lambda = 100$, $C = 60$), λ ($T = 500$, $C = 60$), and C ($T = 500$, $\lambda = 100$).

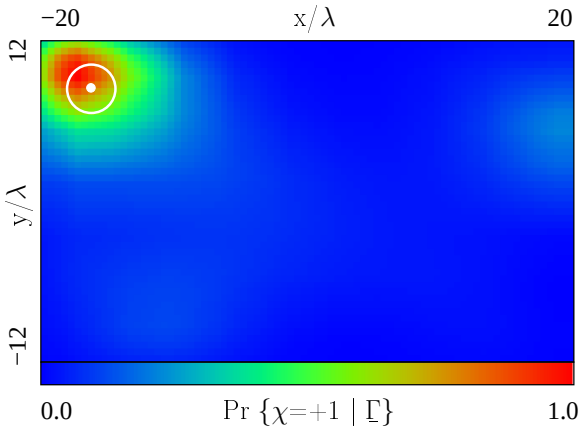

(*a*)

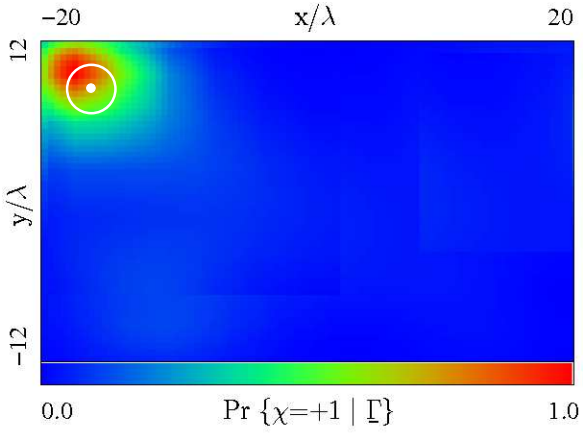

(*b*)

Fig. 4 - *Single-target localization - Outdoor Scenario* - Probability maps of the investigation region D obtained when the test data (*a*) belongs and (*b*) does not belong to the training data set.

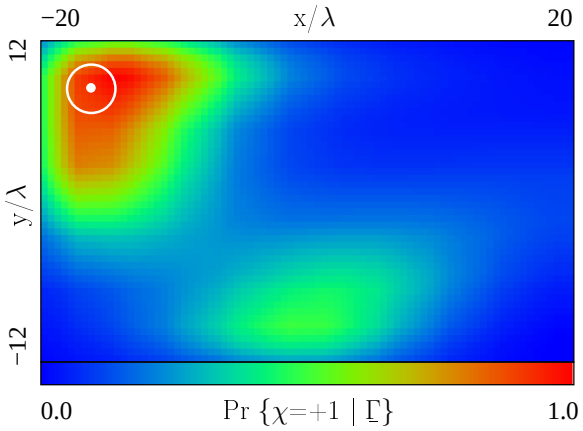

(*a*)

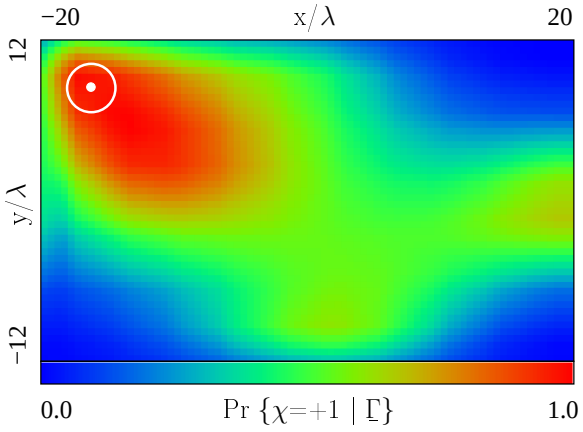

(*b*)

Fig. 5 - *Single-target localization - Indoor Scenario* - Probability maps of the investigation region D obtained when the test data (a) belongs and (b) does not belong to the training data set.

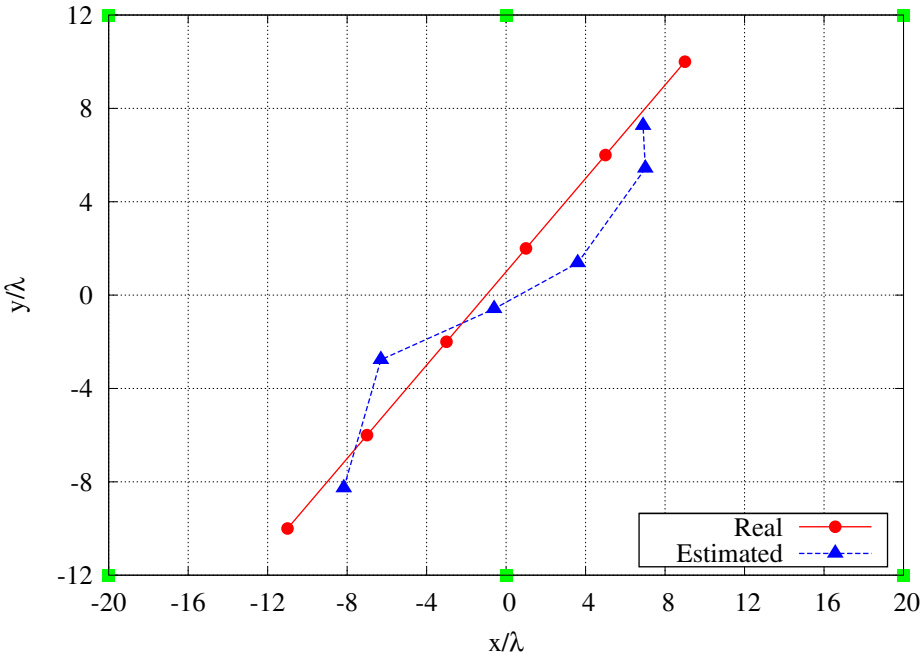

Fig. 6 - *Single-target tracking - Outdoor Scenario* - Actual and estimated trajectories.

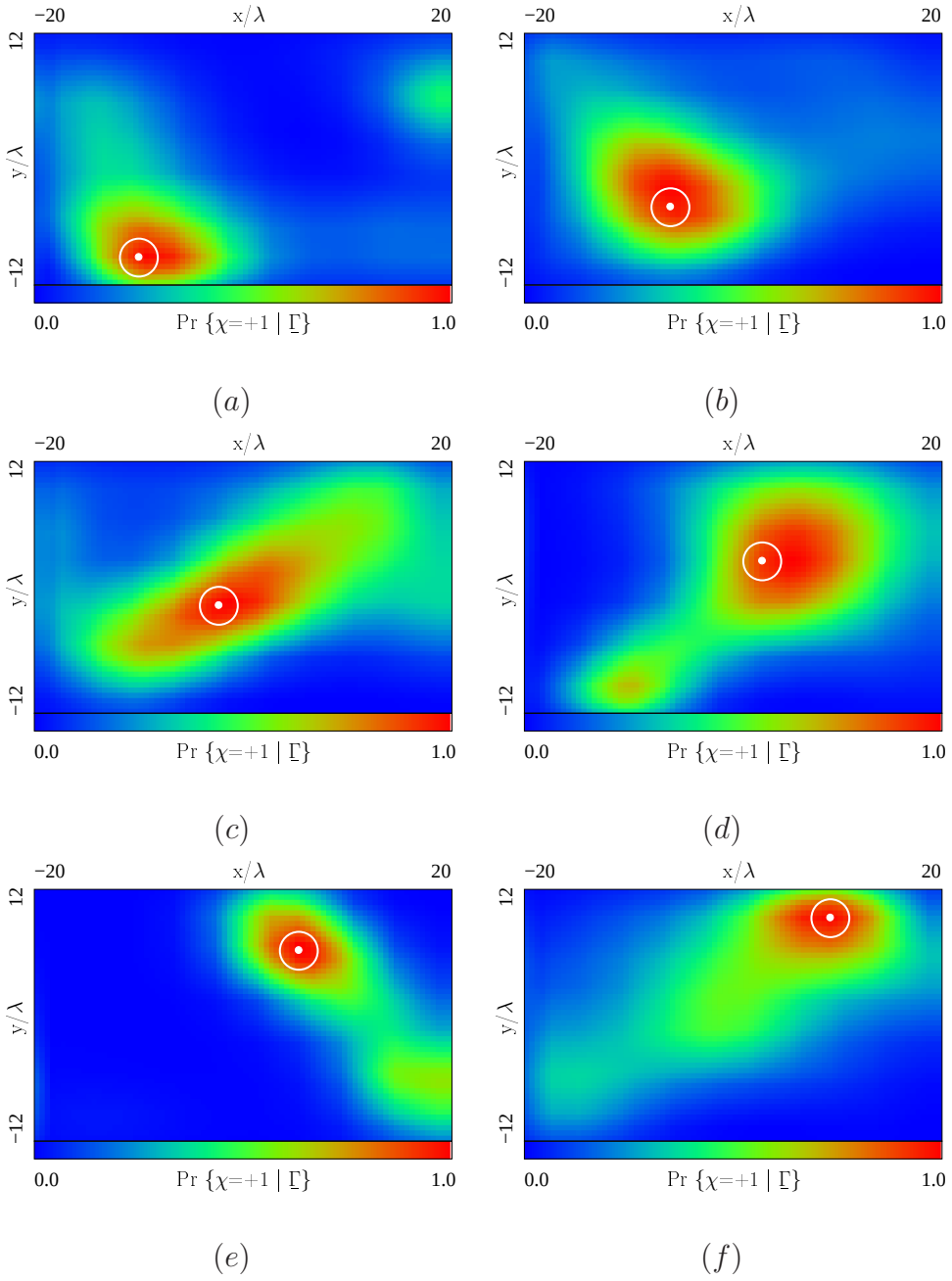

Fig. 7 - *Single-target tracking - Outdoor Scenario* - Screenshots of the probability map of the investigation region D acquired during the target motion.

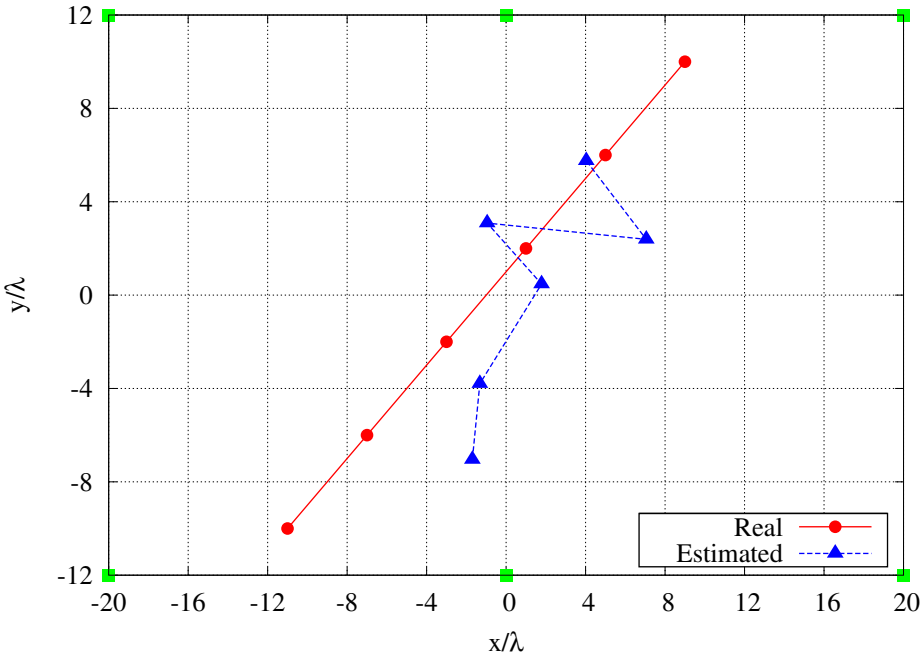

Fig. 8 - *Single-target tracking - Indoor Scenario* - Actual and estimated trajectories.

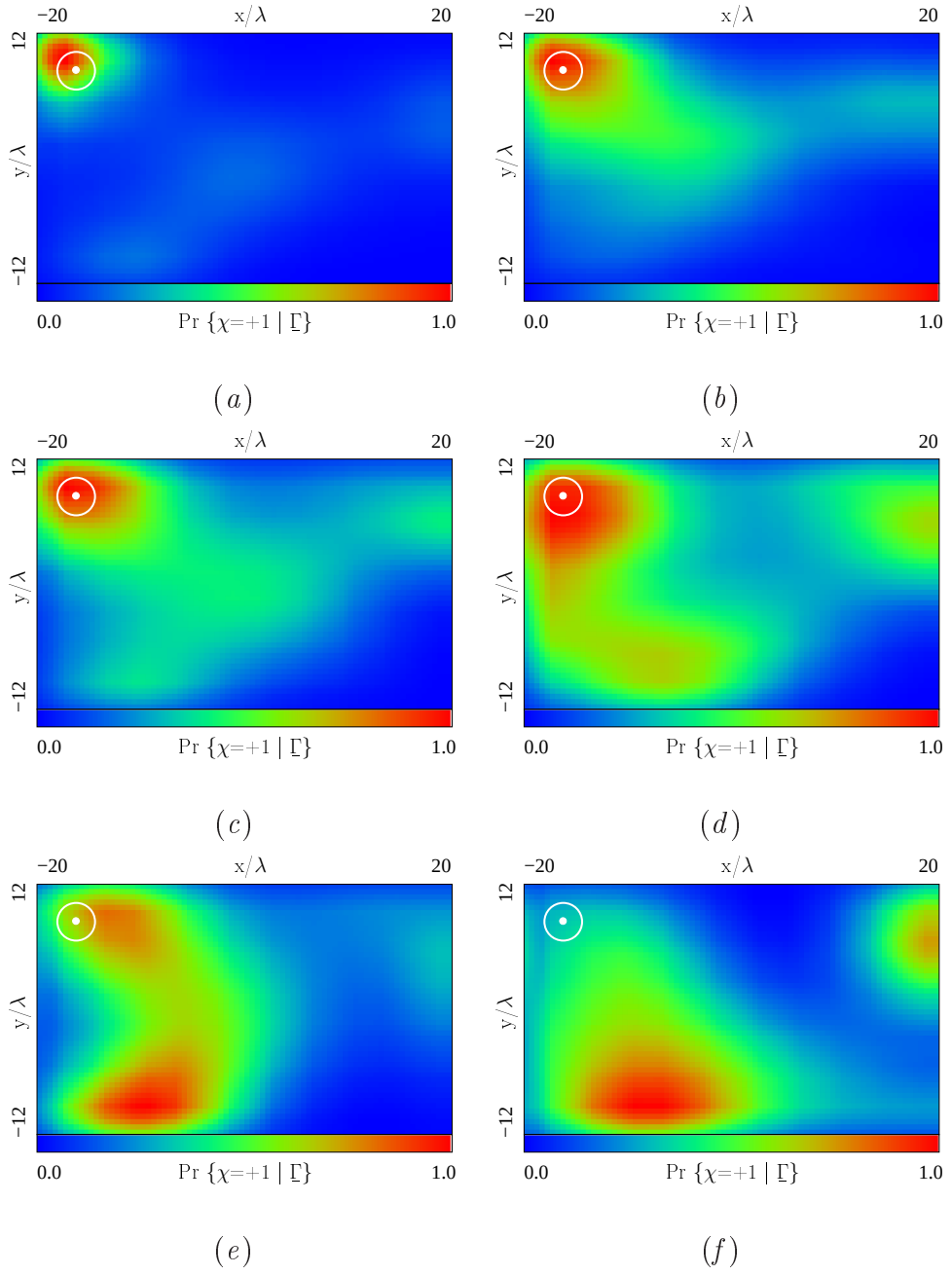

Fig. 9 - *Single-target localization - Outdoor Scenario* ($T_1 \in [0, 500]$, $T_2 \in [0, 500]$, $\lambda = 100$, $C = 60$) - Probability maps of the investigation region D when using (a) $100\%T_1$ and $0\%T_2$, (b) $80\%T_1$ and $20\%T_2$, (c) $60\%T_1$ and $40\%T_2$, (d) $40\%T_1$ and $60\%T_2$, (e) $20\%T_1$ and $80\%T_2$, and (f) $0\%T_1$ and $100\%T_2$ of samples in the training phase.

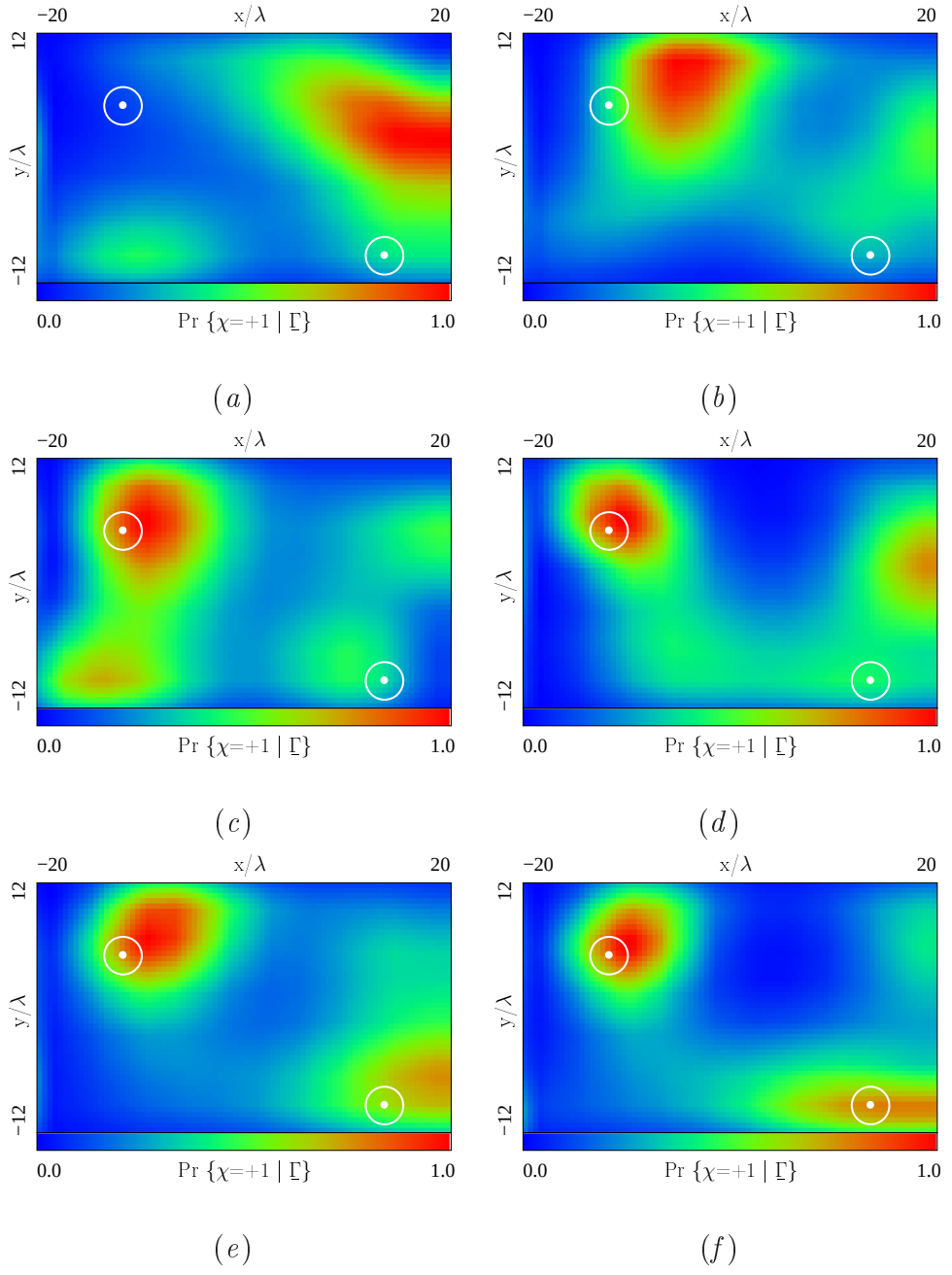

Fig. 10 - *Multiple-targets localization - Outdoor Scenario* ($T_1 \in [0, 500]$, $T_2 \in [0, 500]$, $\lambda = 100$, $C = 60$) - Probability maps of the investigation region D when using (a) $100\%T_1$ and $0\%T_2$, (b) $80\%T_1$ and $20\%T_2$, (c) $60\%T_1$ and $40\%T_2$, (d) $40\%T_1$ and $60\%T_2$, (e) $20\%T_1$ and $80\%T_2$, and (f) $0\%T_1$ and $100\%T_2$ of samples in the training phase.

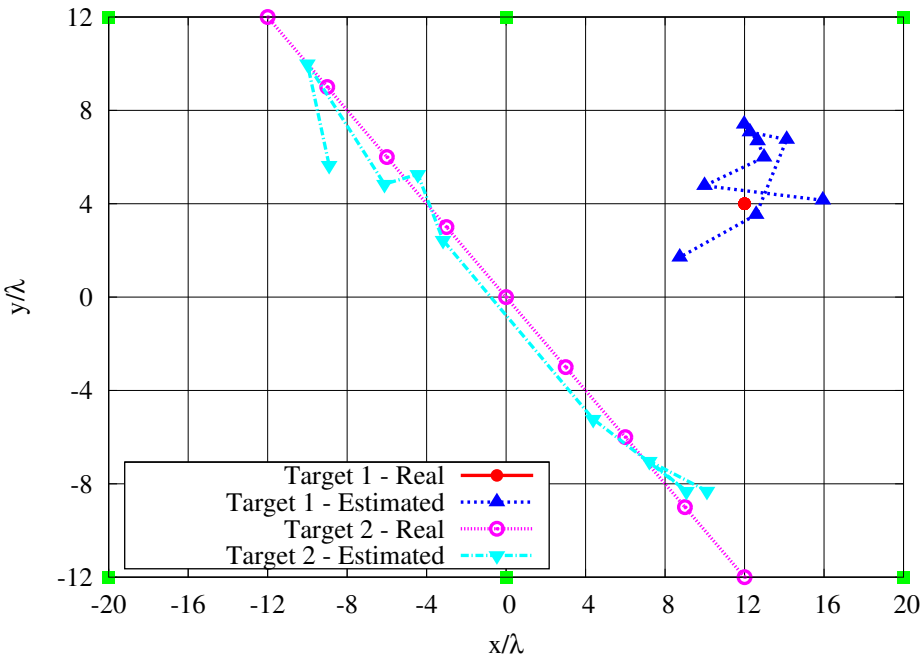

Fig. 11 - *Multiple-targets tracking - Outdoor Scenario* - Actual and estimated trajectories.

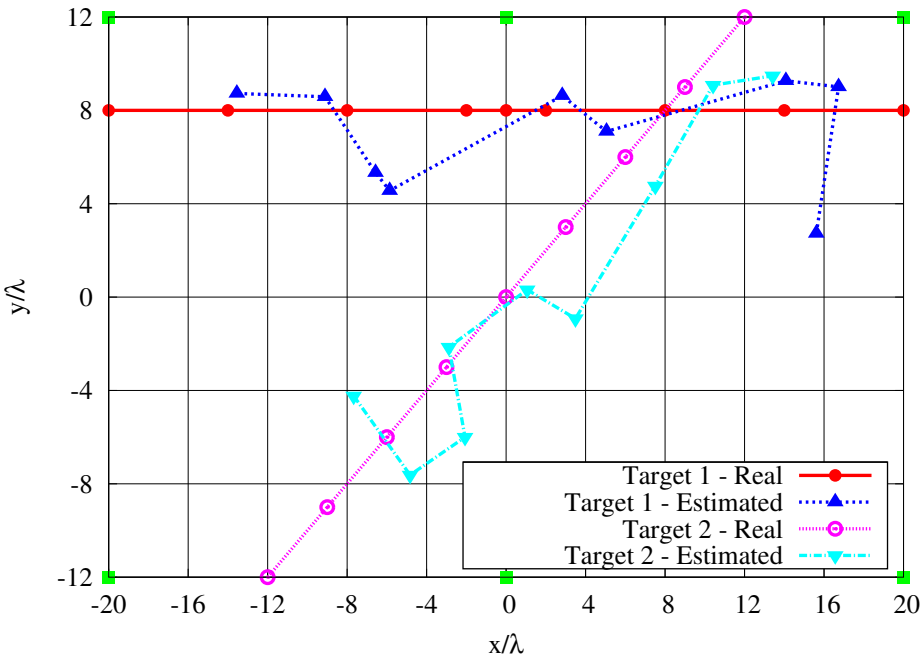

Fig. 12 - *Multiple-targets tracking - Outdoor Scenario* - Actual and estimated trajectories.

	Outdoor		*Indoor*	
Time Instant	ρ	$\rho \times \rho_{max}$ $[\lambda]$	ρ	$\rho \times \rho_{max}$ $[\lambda]$
1	0.071	3.32	0.209	9.76
2	0.070	3.30	0.131	6.09
3	0.060	2.78	0.115	5.38
4	0.057	2.67	0.048	2.23
5	0.045	2.09	0.089	4.15
6	0.074	3.46	0.140	6.53
Average Error : $\overline{\rho}$	0.063	2.94	0.122	5.69

Tab. I - *Single-target tracking* - Localization errors for the outdoor and the indoor scenarios.

	$Single\,Target$		$Multiple\,Target$			
	$j=1$		$j=1$		$j=2$	
	ρ	$\rho \times \rho_{max}$ $[\lambda]$	ρ	$\rho \times \rho_{max}$ $[\lambda]$	ρ	$\rho \times \rho_{max}$ $[\lambda]$
(a)	0.044	2.07	0.217	10.12	0.158	7.37
(b)	0.059	2.77	0.196	9.14	0.135	6.31
(c)	0.093	4.34	0.151	7.02	0.074	3.44
(d)	0.150	6.98	0.149	6.96	0.062	2.91
(e)	0.262	12.23	0.063	2.93	0.106	4.94
(f)	0.357	16.67	0.031	1.46	0.063	2.93

Tab. II - *Multiple-targets localization - Outdoor Scenario* - Localization errors for the single and multiple target case.